Supplementary Materials for

Thermal transport across copper-water interface from deep potential molecular dynamics

Zhiqiang Li[a], Xiaoyu Tan[b], Zhiwei Fu[b,c], Linhua Liu[a,b,*], Jia-Yue Yang[a,b,*]

[a]*Optics & Thermal Radiation Research Center, Institute of Frontier and Interdisciplinary Science, Shandong University, Qingdao, Shandong 266237, China*

[b]*School of Energy and Power Engineering, Shandong University, Jinan, Shandong 250061, China*

[c]*Science and Technology on Reliability Physics and Application of Electronic Component Laboratory, The 5th Electronics Research Institute of the Ministry of Industry and Information Technology, Guangzhou 511370, China*

SI. Validation tests

To test the accuracy of DLP in a large system, we enlarge the original system (139 atoms) along the x- and z-directions four times into a large system (2224 atoms). Both small and large systems were simulated at 300K in the NVT ensemble, for 0.65 ns with a time step of 0.5 fs. We analyzed the average values of the density and radial distribution function (RDF) within the last 0.55 ns. Fig. S1 shows an excellent agreement for RDF between the large system and the small system. Therefore, we conclude that the trained DLP could generalize the accuracy of DFT to a larger system.

*Author to whom correspondence should be addressed. E-Mail: jy_yang@sdu.edu.cn (J.Y.), liulinhua@sdu.edu.cn (L.L.)

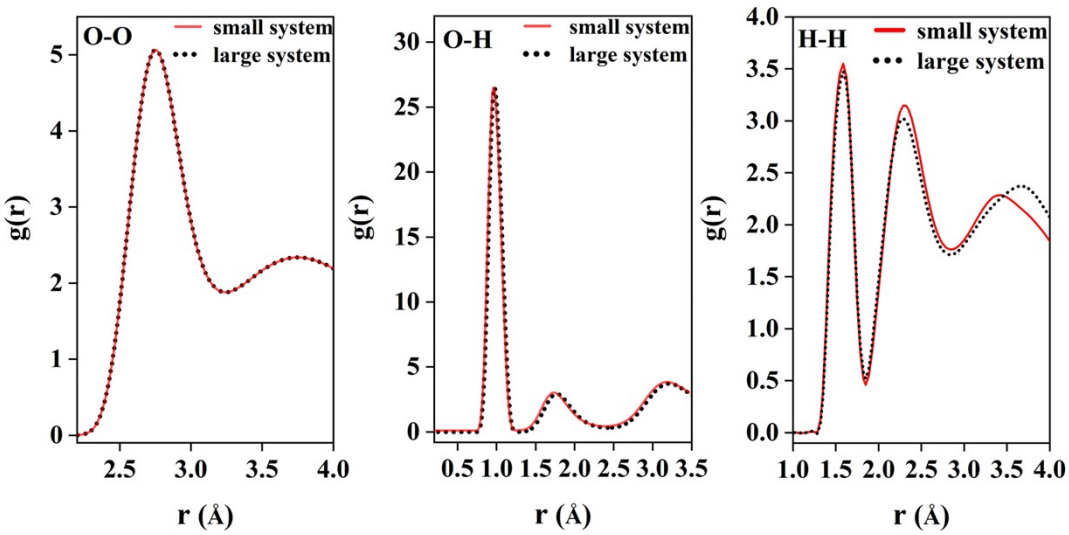

Fig. S1 Comparison of the RDFs of water obtained from DPMD simulations between small system and large system. The red line represents the small system, and the black dashed line represents the large system.

SII. LJ potential model

The generally accepted Lennard-Jones (LJ) potential model coupling with the coulomb interaction is employed to describe the atomic interactions in the CMD simulations. The specific expression is as follows:

$$u_{ij}=\frac{q_i q_j}{4\pi\varepsilon_0 r_{ij}}+4\varepsilon_{ij}\left[\left(\frac{\sigma_{ij}}{r_{ij}}\right)^{12}-\left(\frac{\sigma_{ij}}{r_{ij}}\right)^{6}\right] \quad \backslash*$$

MERGEFORMAT (1)

where r_{ij} is the distance between atom i and atom j. u_{ij} represents the interaction energy. ε_{ij} and σ_{ij} are energy parameters and length parameters, respectively. q_i is the charge of the i-th particle and ε_0 is the vacuum permittivity.

And the simulation results will be compared with DPMD simulations. Detailed potential parameters are summarized in Table I, and the parameters between copper and oxygen are determined by the Lorentz−Berthelot mixing rule[1]. The formula is as follows:

$$\sigma_{Cu-O} = \frac{\sigma_{Cu} + \sigma_{o}}{2} \quad \backslash*$$

MERGEFORMAT (2)

$$\varepsilon_{Cu-O} = \left(\varepsilon_{Cu} \varepsilon_{O}\right)^{0.5} \quad \backslash*$$

MERGEFORMAT (3)

The particle-particle-particle mesh (PPPM) method[2] with an accuracy of 1.0×10^{-4} was served to solve long-range interactions. The SHAKE algorithm was performed to ensure the rigidity of the water molecules. As for the cutoff distance, it is set to 10 Å.

It is noted that CMD simulation adopts the same setup details as DPMD simulation.

Table I. potential energy and related parameters between particles

Model	Parameters	Values	Units
TIP4P	ε_{O-O}	0.00672	eV
	σ_{O-O}	3.1536	Å
	q_H	0.52	e
	q_O	−1.04	e
SPC	ε_{O-O}	0.00673	eV
	σ_{O-O}	3.166	Å
	q_H	0.41	e
	q_O	-0.82	e
Cu	ε_{Cu-Cu}	0.4096	eV
	σ_{Cu-Cu}	0.233	nm

SIII. Generation of the Training Sets by DP-GEN

The training sets are generated using the DP-GEN software package, consisting of three steps, exploration, labeling, and training, as shown in Fig. S2. Initial training datasets are extracted from the AIMD simulation using PAW method and PBE functional. The AIMD simulations contains two steps: Firstly, the initial structure was optimized using the Conjugate-Gradient (CG) algorithm.

Secondly, the structures were relaxed at 300 K in the canonical ensemble (NVT) with a time step of 1 fs. The cutoff energy for the plane wave expansion is set to be 550 eV, and the Brillouin zone is sampled at the Γ point. The SCF energy convergence threshold was chosen to be 10^{-6} Hartree/atom. Simulation runs at 300K in the NVT ensemble, for 4000 steps with a time step of 0.5 fs. Based on the initial training sets, we trained an initial deep potential model for later configuration explorations and labeling. Next, new configurations from DPMD simulations will be added to the training sets for a new round of training. Finally, a relatively accurate and reliable potential model will be constructed after several above cycles.

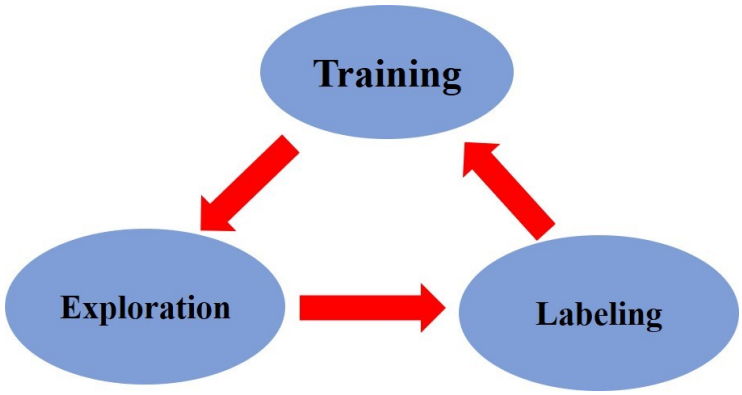

Fig. S2 Workflow of DP-GEN

SIV. The effect of the thermal bath type, temperature and system size on the ITC

Here, we investigated the effect of the thermal bath type, temperature and system size on the interfacial thermal conductance. The same system size and simulation details as in the manuscript were used.

Thermal Bath Type

The literature[3] shows that the thermal bath type has an effect on the interfacial heat transfer, we performed DPMD simulation using nosé-hoover thermostat and the calculated results were compared with the results of this paper (Langevin thermostat), as shown in the Fig. S3. According

to the equation (7) in the manuscript, we calculated the ITC at the interface. As shown in the Table II, the ITC calculated using nosé-hoover thermostat is smaller than the results by langevin thermostat.

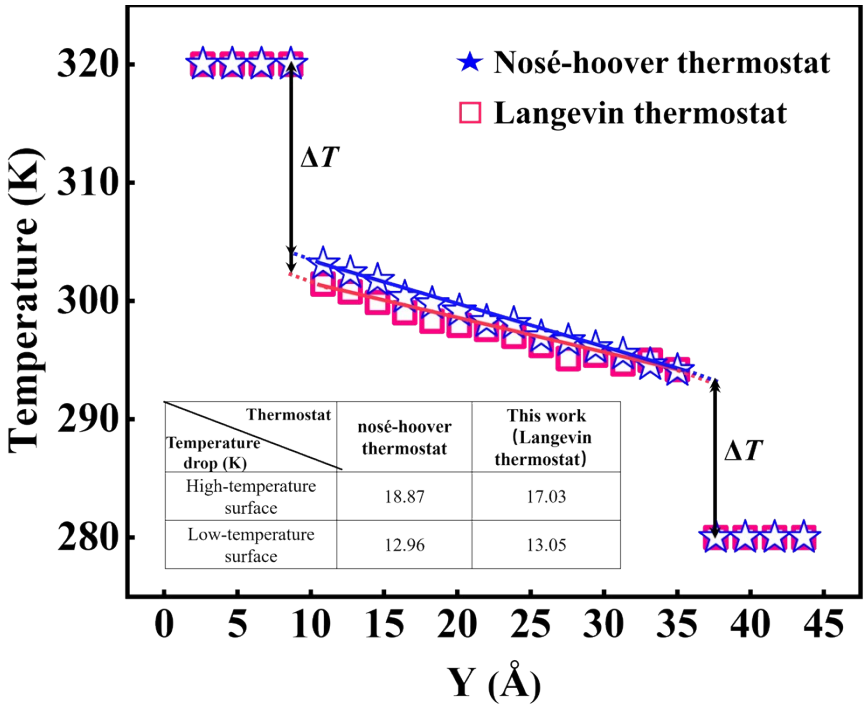

Fig. S3 The temperature distributions along the y direction calculated from dynamical simulations with nosé-hoover thermostat and langevin thermostat, respectively. The table in the figure shows the temperature drop at the high and low temperature surfaces.

Table II. ITC predicted using different thermostat. ITC is in units of $W/m^2 \cdot K$.

Thermostat / ITC	langevin thermostat	nosé-hoover thermostat
High-temperature interface	2.17×10^8	1.15×10^8
Low-temperature interface	2.84×10^8	1.67×10^8

Average value	$(2.505 \pm 0.335)\times10^{8}$	$(1.410 \pm 0.260)\times10^{8}$

Temperature Effect

To investigate the effect of temperature on ITC, we calculated the ITC at 290 K, 300K and 310 K, respectively. The bottom plate was heated up to 320 K, 310K and 300 K, respectively to create a temperature gradient. The temperature of the top plate remained at 300 K, 290 K and 280 K, respectively. Note that the ITC at 300 K is calculated by the temperature difference of 20 K, which is different from the result in the manuscript (the temperature difference of 40 K). Fig. S4 shows the temperature profiles and temperature drop. As shown in the Table III, the ITC increases with rising temperature. Specially, the ITC of high-temperature interface at 300 K is less than that of 290 K and 310 K, and the ITC of low-temperature interface at 300 K lies between 290K and 310K. The reason for this is the difference in temperature difference and the statistical averaging process. Combined with the results in the manuscript, in our view, the ITC should follow the trend of increasing with temperature, in agreement with the result of Fig. 5 in the literature[4].

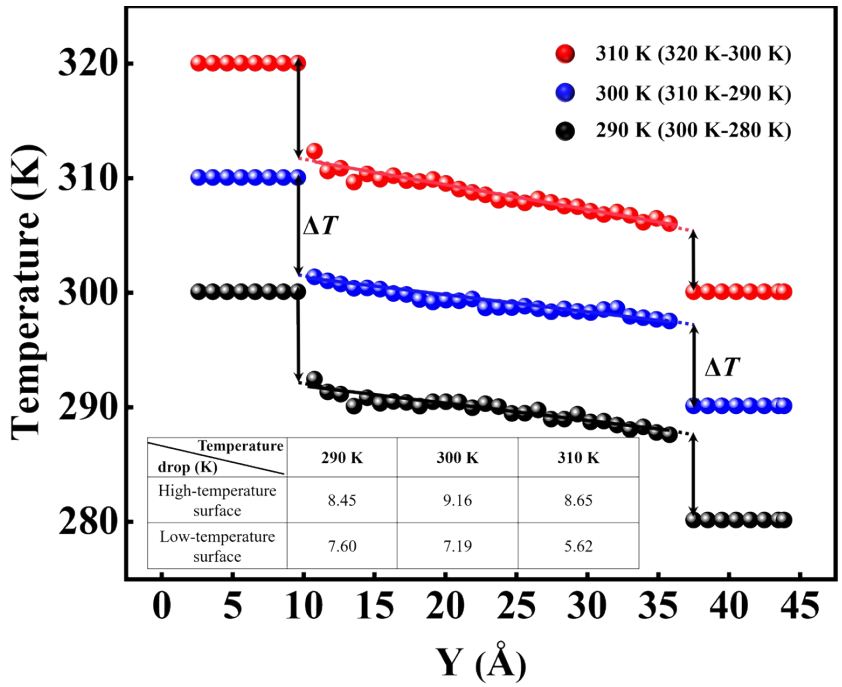

Fig. S4 The temperature distributions along the y direction calculated from dynamical simulations at 290 K, 300 K and 310 K, respectively. The table in the figure shows the temperature drop at the high and low temperature surfaces.

Table III. ITC predicted at different temperature. ITC is in units of $W/m^2 \cdot K$.

Temperature / ITC	290 K	300 K	310 K	This work (300 K)
High-temperature interface	2.02×10^8	1.95×10^8	2.29×10^8	2.17×10^8
Low-temperature interface	2.25×10^8	2.48×10^8	3.52×10^8	2.84×10^8
Average value	$(2.135 \pm 0.115)\times10^8$	$(2.215 \pm 0.265)\times10^8$	$(2.905 \pm 0.615)\times10^8$	$(2.505 \pm 0.335)\times10^8$

System Size

Size effect has been a challenge for NEMD simulations. Here, we investigate the effect of different

111 cross-sectional area and system length on interfacial thermal conductance. The main findings are

112 presented in Table IV and Fig. S5. As shown in the Table IV, the average ITC and the ITC at low-

113 temperature interface tend to increase with rising cross-sectional area and to decrease with rising

114 channel height. As for the ITC at high-temperature interface, the trend is not particularly obvious,

115 and the additional calculations are needed to perform.

116

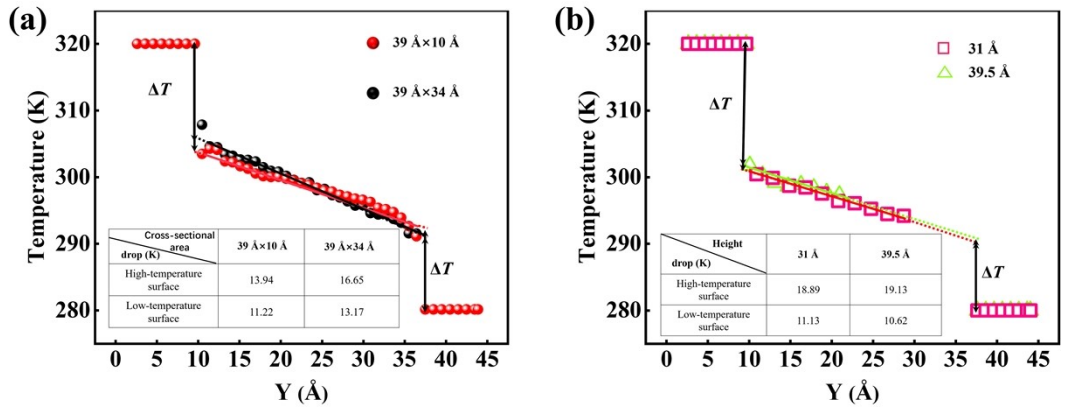

Fig. S5 (a) The temperature distributions along the y direction calculated from dynamical simulations with different cross-sectional area. (b) the temperature distributions along the y direction calculated from dynamical simulations with different channel height. The table in the figure shows the temperature drop at the high and low temperature surfaces.

117

118 Table IV. ITC predicted with different size. ITC is in units of $W/m^2 \cdot K$

Size / ITC	Cross-sectional area (Å^2)			Channel Height (Å)		
	39 ×10	39 ×25	39 ×34	31	39.5	46.5
High-temperature interface	2.02×10^8	1.95×10^8	2.73×10^8	2.41×10^8	2.04×10^8	2.17×10^8
Low-temperature	2.25×10^8	2.48×10^8	4.70×10^8	4.09×10^8	3.67×10^8	2.84×10^8

interface						
Average value	(2.135 ± 0.115)×10^8	(2.215 ± 0.265)×10^8	(3.715 ± 0.985)×10^8	(3.25 ± 0.840)×10^8	(2.855 ± 0.815)×10^8	(2.505 ± 0.335)×10^8

In summary, it can be concluded that size, temperature and thermostat all expert an effect on the interfacial thermal conductance, and more exploration is needed. In addition, previous computational and experimental studies demonstrated a proportional relation between work of solid-liquid adhesion or solid-liquid interaction strength and interfacial thermal conductance (ITC). This presents the idea to design different coating surfaces for modulating the interfacial thermal conductance. Then, a reliable interfacial thermal conductance can be calculated based on the accurate machine learning potential.

References

1 D. Boda and D. Henderson, The effects of deviations from Lorentz–Berthelot rules on the properties of a simple mixture, *Molecular Physics*, 2008, **106**, 2367–2370.

2 J. V. L. Beckers, C. P. Lowe and S. W. De Leeuw, An Iterative PPPM Method for Simulating Coulombic Systems on Distributed Memory Parallel Computers, *Molecular Simulation*, 1998, **20**, 369–383.

3 Z. Li, S. Xiong, C. Sievers, Y. Hu, Z. Fan, N. Wei, H. Bao, S. Chen, D. Donadio and T. Ala-Nissila, Influence of thermostatting on nonequilibrium molecular dynamics simulations of heat conduction in solids, *J. Chem. Phys.*, 2019, **151**, 234105.

4 J. Diao, D. Srivastava and M. Menon, Molecular dynamics simulations of carbon nanotube/silicon interfacial thermal conductance, *The Journal of Chemical Physics*, 2008, **128**, 164708.